CrystEngComm

View Online
Dynamic Article Links

Cite this: *CrystEngComm*, 2011, **13**, 2430

www.rsc.org/crystengcomm

PAPER

Coexistence of two donor packing motifs in the stable molecular metal α-'pseudo-κ'-(BEDT-TTF)$_4$(H$_3$O)[Fe(C$_2$O$_4$)$_3$]·C$_6$H$_4$Br$_2$†

Leokadiya V. Zorina,*[a] Salavat S. Khasanov,[a] Sergey V. Simonov,[a] Rimma P. Shibaeva,[a] Vladimir N. Zverev,[a] Enric Canadell,[b] Tatiana G. Prokhorova[c] and Eduard B. Yagubskii[c]

Received 1st November 2010, Accepted 5th January 2011
DOI: 10.1039/c0ce00804d

The crystal and electronic structure of a new radical cation salt α-'pseudo-κ'-(BEDT-TTF)$_4$H$_3$O[Fe(C$_2$O$_4$)$_3$]·C$_6$H$_4$Br$_2$ have been studied. The new triclinic crystals contain two conducting organic layers which are characterized by different BEDT-TTF packing motifs: a 'pseudo-κ'-layer which is composed of charged dimers and neutral monomers of BEDT-TTF orthogonal to each other and an α-layer which consists of inclined, uniformly charged BEDT-TTF stacks. According to electronic band structure calculations, the 'pseudo-κ' layer has a large gap between the HOMO bands at the Fermi level and should be associated with an activated conductivity. In contrast, the α-layer is a strongly two-dimensional electronic system with uniform intermolecular interactions. The absence of any nesting in the Fermi surface of the α-layer suggests that this salt should be a stable metal down to low temperatures. Metallic properties have been observed in the crystals in the 300–0.4 K temperature range. Besides, well pronounced Shubnikov–de Haas oscillations of the magnetoresistance have been revealed at $B > 8$ T. The salt investigated is a new phase in the (BEDT-TTF)$_4$A^{I}[M^{III}(C$_2$O$_4$)$_3$]G family of organic molecular conductors with paramagnetic anions and different guest solvent molecules G in the anion layer. Structural features of the new α-'pseudo-κ'-crystals and other known phases of the family (β″, 'pseudo-κ' and α-β″) have been compared.

Introduction

A family of the radical cation salts with magnetic tris(oxalato)metallate anions of (BEDT-TTF)$_4$A^{I}[M^{III}(C$_2$O$_4$)$_3$]·G composition, where BEDT-TTF is bis(ethylenedithio)tetrathiafulvalene; A^{I} is NH$_4^+$, K$^+$, H$_3$O$^+$, Rb$^+$; M^{III} is Fe, Cr, Mn; G is a guest solvent molecule,[1–18] represents an important class of modern hybrid multifunctional materials. In a seminal article[1] published in 1995 it has been demonstrated for the first time that superconductivity of organic donor layers and paramagnetism of anion sublattice coexist in β″-(BEDT-TTF)$_4$H$_3$O[Fe(C$_2$O$_4$)$_3$]·C$_6$H$_5$CN. The high interest on the (BEDT-TTF)$_4$A^{I}[M^{III}(C$_2$O$_4$)$_3$]·G family is connected with the flexibility of this four-component tunable system whose crystals can be widely modified by variation of A^{I}, M^{III} and G constituents and exhibit both isomorphism and polymorphism. Up to date, three series of salts with different packing modes of conducting BEDT-TTF layers, β″, 'pseudo-κ' and α-β″, have been synthesized. It is remarkable that a neutral solvent G, involved as a guest molecule into the anion layer, plays a great role in these molecular compounds essentially affecting both crystal structure and transport properties of the crystals. On the one hand, solvent substitution can cause changes of the polymorph modification or stoichiometry of the salts. On the other hand, the same crystal phase can exist with a wide range of the solvents and even their mixtures in varied proportions keeping the general crystal packing mode. Conductivity of the crystals and/or the temperature of the superconducting transition in both cases strongly depend on the shape, size, chirality and composition of the G solvent.

In a recent article[18] we analyzed the effect of electrocrystallization medium on structure and conducting properties of single crystals of the (BEDT-TTF)$_4$H$_3$O$^+$[Fe^{III}(C$_2$O$_4$)$_3$]·G family. As a part of the work, synthesis of a novel triclinic phase in the family with G = 1,2-dibromobenzene was described. The crystals contain alternating α- and 'pseudo-κ' BEDT-TTF layers, this coexistence having never been observed before in molecular conductors, and show a metallic behavior down to 0.4 K. Here we report the crystal and electronic structure of the novel α-'pseudo-κ'-(BEDT-TTF)$_4$H$_3$O[Fe(C$_2$O$_4$)$_3$]·C$_6$H$_4$Br$_2$ phase and a detailed structural comparison with known β″, 'pseudo-κ'

[a]*Institute of Solid State Physics, RAS, Chernogolovka, MD, 142432, Russia. E-mail: zorina@issp.ac.ru*
[b]*Institut de Ciència de Materials de Barcelona, CSIC, Campus de la UAB, E-08193 Bellaterra, Spain*
[c]*Institute of Problems of Chemical Physics, RAS, Chernogolovka, MD, 142432, Russia*

† Electronic supplementary information (ESI) available. CCDC reference number 799269. For ESI and crystallographic data in CIF or other electronic format see DOI: 10.1039/c0ce00804d

and α-β″ phases of the family and with several other bi-layered radical cation salts. The band structure and Fermi surface of the metallic α-layer in the title crystal are compared with those of the α-(BEDT-TTF)$_2$MHg(SCN)$_4$ family[19,20] and drastic differences between them are discussed.

Experimental

X-Ray diffraction

Single crystal X-ray structural study was carried out at room temperature and 120 K using an Oxford Diffraction Gemini-R diffractometer equipped with a Ruby CCD detector. Experimental data collections were performed with MoK_α radiation [λ(MoK_α) = 0.71073 Å, graphite monochromator, ω-scans]. Data reduction with empirical absorption correction of experimental intensities (Scale3AbsPack program) was made with the CrysAlisPro software.[21]

The structure was solved by a direct method followed by Fourier syntheses and refined by a full-matrix least-squares method using the SHELX-97 programs[22] in an anisotropic approximation for all non-hydrogen atoms. H-atoms in BEDT-TTF and dibromobenzene molecules were placed in idealized positions and refined using a riding model, U_{iso}(H) was fixed at 1.2U_{eq}(C). Coordinates of the H-atoms in the hydroxonium H_3O^+ cations were found from difference electron density map and refined with U_{iso}(H) = 1.5U_{eq}(O), O–H bond lengths being restrained to equal value with standard deviation of 0.02 Å (SADI instruction).

Crystal data. $C_{52}H_{39}Br_2FeO_{13}S_{32}$, M = 2113.42, T = 120(1) K, triclinic, a = 10.2479(4), b = 19.6937(9), c = 36.3999(15) Å, α = 88.258(3), β = 88.801(3), γ = 89.558(4)°, V = 7341.0(5) Å^3, $P\bar{1}$, Z = 4, D_{calc} = 1.912 g cm^{-3}, μ = 22.64 cm^{-1}, $2\Theta_{max}$ = 55.76°, reflections measured 71 867, unique reflections 34 493 (R_{int} = 0.0648), reflections with $I > 2\sigma(I)$ = 19 188, parameters refined 1823, R_1 = 0.0554, wR_2 = 0.1067, GOF = 1.000. Unit cell parameters at room temperature have been published earlier.[18]

Electronic band structure calculations

The tight-binding band structure calculations[23] were of the extended Hückel type. A modified Wolfsberg–Helmholtz formula was used to calculate the non-diagonal $H_{\mu\nu}$ values.[24] All valence electrons were taken into account in the calculations and the basis set consisted of Slater-type orbitals of double-ζ quality for C 2s and 2p, S 3s and 3p and of single-ζ quality for H. The ionization potentials, contraction coefficients and exponents were taken from previous work.[25,26]

Conductivity and magnetotransport measurements

The transport measurements in the temperature range (0.4–300 K) were carried out in a cryostat with a superconducting solenoid, which generated magnetic field of up to 17.2 T. The temperature dependences of the electrical resistance of single crystals were measured using a four-probe technique by a lock-in detector at 20 Hz alternating current J = 1 mkA. Two contacts were attached to each of two opposite sample surfaces with conducting graphite paste. In the experiment we have measured the out-of-plane resistance $R_\perp$ with the current running perpendicular to conducting layers. Because of the high anisotropy of the samples we did not succeed in the measurements of the in-plane sample resistance.

Results and discussion

Crystal structure

Single crystals of α-'pseudo-κ'-(BEDT-TTF)$_4$H$_3$O[Fe(C$_2$O$_4$)$_3$]·C$_6$H$_4$Br$_2$ have triclinic $P\bar{1}$ symmetry and a layered structure (Fig. 1). Conducting BEDT-TTF layers alternate along the c-direction with complex anion layers which include paramagnetic [Fe^{III}(C$_2$O$_4$)$_3$]$^{3-}$ anions, H_3O^+ cations and neutral dibromobenzene molecules. The asymmetric unit contains eight BEDT-TTF donor molecules (A–H), two anions, two hydroxonium cations and two solvent molecules, all in general positions; the atomic numbering scheme is shown in the ESI†. The structure comprises two identical anion layers and two crystallographically unique BEDT-TTF layers per unit cell. Room temperature and 120 K structures differ mainly by the degree of disorder in conducting layers: at room temperature the outer ethylene groups of BEDT-TTF molecules have large thermal displacement parameters while at 120 K only one ethylene fragment of one BEDT-TTF remains disordered. Since the structure quality at low temperature is much better than at room temperature,

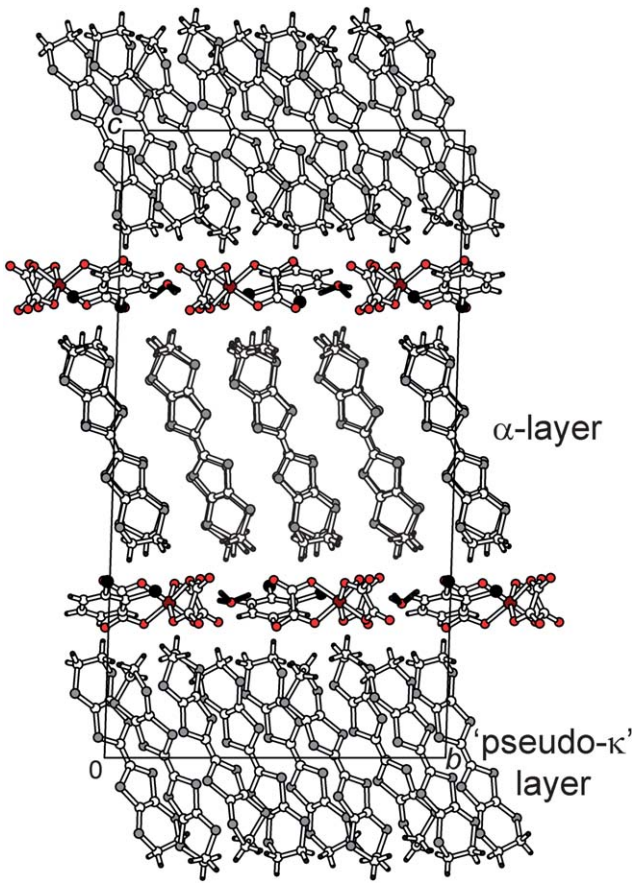

Fig. 1 A view of the α-'pseudo-κ'-(BEDT-TTF)$_4$H$_3$O[Fe(C$_2$O$_4$)$_3$]C$_6$H$_4$Br$_2$ structure along the a-axis.

only the 120 K data have been analyzed in detail and deposited in CCDC.

Two independent conducting organic layers, which are repeated alternately along the *c*-axis, differ from each other by type of molecular packing and distribution of the positive charge between BEDT-TTF molecules. Four molecules A, B, C and D are arranged into the layer at $z = 0$ (Fig. 2a). The A and C molecules make two independent centrosymmetric dimers (dark molecules in Fig. 2a) with small intradimer interplanar separations of 3.38(1) and 3.37(1) Å, respectively. The A and C dimers are rotated by 87.02(3)° with respect to each other. The dimers are surrounded by single B and D molecules (light-colored BEDT-TTFs in Fig. 2a) which make the dihedral angles of 73.91(3) with each other and 80.22(3) and 80.93(3)° with the A and C dimers, respectively. All the A–D molecules at 120 K are completely ordered in an eclipsed conformation. Central C=C valence bonds in TTF fragments which are sensitive to the charge state of BEDT-TTF show significant charge difference between pairs of A, C and B, D molecules: the corresponding bond lengths amount to 1.402(6), 1.384(6) and 1.348(6), 1.352(6) Å, respectively. Together with essential planarity of the first pair of the molecules and strong deviation from the planarity of the second pair (dihedral angles of molecular bending across the inner sulfur atoms of BEDT-TTF are 2.31(3)–2.92(4)° for A, C against 9.37(3)–9.85(3)° for B, D), this indicates that dimerized A and C radical cations accumulate all the positive charge within the layer while B and D molecules are essentially neutral. This type of packing from charged $[(BEDT\text{-}TTF)_2]^{2+}$ dimers surrounded by orthogonal neutral $BEDT\text{-}TTF^0$ monomers was described earlier in the orthorhombic $(BEDT\text{-}TTF)_4A[M(C_2O_4)_3]PhCN$ ($M = Fe^{III}$, $A = K^+$ or NH_4^+; $M = Cr^{III}$, $A = H_3O^+$) crystals of the same stoichiometry and named 'pseudo-κ' type.[1,4] The crystals of the pure 'pseudo-κ' orthorhombic phase are semiconductors due to strong charge localization inside the dimers, and the same semiconducting properties can be expected for the similarly dimerized 'pseudo-κ' layer in the new mixed α-'pseudo-κ' crystals. There is a large number of intermolecular contacts of S···S type inside the dimers equal to 3.436(2)–3.656(2) Å for A and 3.423(2)–3.608(2) Å for C and between dimers and monomers in the range of 3.152(2)–3.693(2) Å while only one slightly shortened contact of 3.612(2) or 3.621(2) Å exists between the neutral B and D molecules.

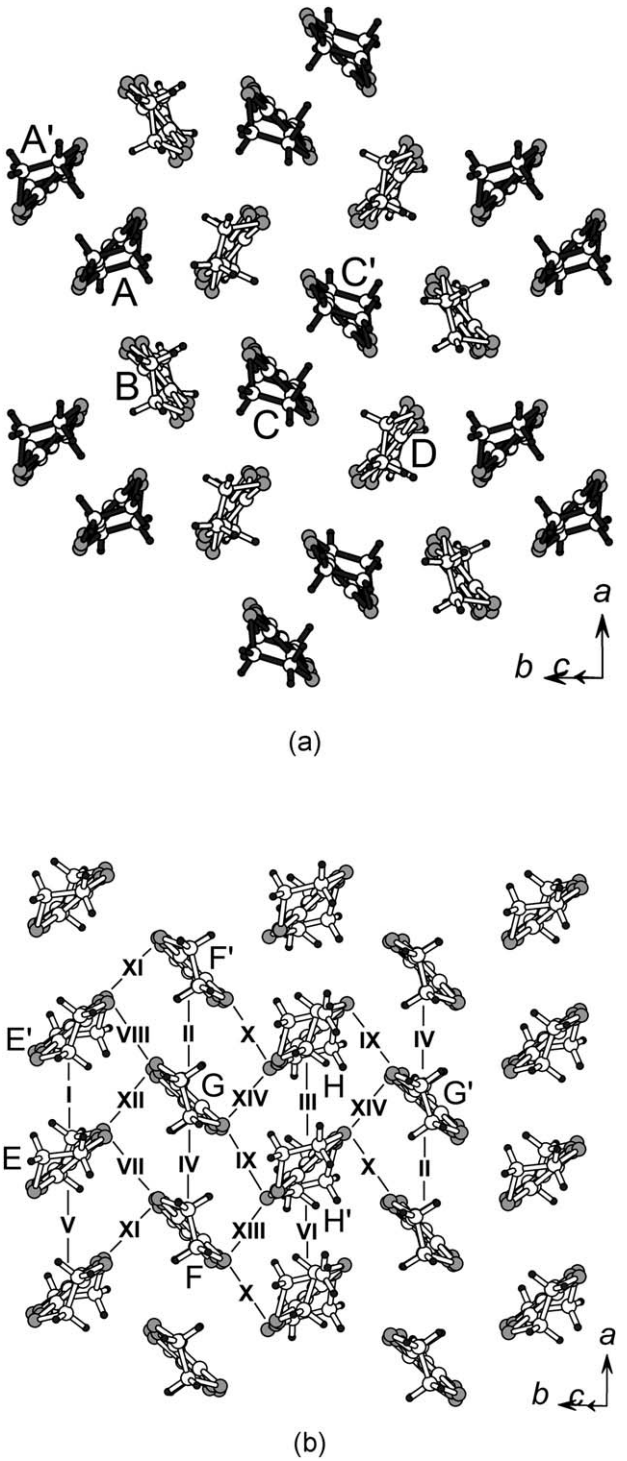

Fig. 2 The conducting BEDT-TTF layers projected along the long molecular axis: (a) the 'pseudo-κ' layer and (b) the α layer.

The other four molecules E, F, G and H lie in the layer centered at $z = 0.5$. The layer has α-type packing motif (Fig. 2b) and contains three independent BEDT-TTF stacks running along the *a*-direction, the molecular planes in adjacent stacks are inclined by 92–97° with respect to each other. Stacks E and H are composed of one molecule (E or H, respectively) while stack FG consists of alternating F and G molecules. All the stacks have large and rather uniform interplanar separations of the adjacent radical cations: 3.85(1) and 3.97(1) Å in the stack E, 3.70(6) and 3.77(6) Å in the stack FG, 3.72(1) and 3.86(1) Å in the stack H. The large angle between the molecular planes and stacking axis (~45°) leads to the almost complete absence of intrastack BEDT-TTF overlaps: only S-atoms of the outer six-membered circles of neighboring donors are overlapping; the longitudinal shift of the BEDT-TTF molecules in the α-layer is zero. All intrastack intermolecular S···S contacts exceed the sum of the van der Waals radii equal to 3.70 Å while there are many interstack S···S contacts in the range of 3.423(2)–3.695(2) Å. The molecule E has a staggered conformation of the outer ethylene groups whereas the F and G molecules have an eclipsed conformation, and H reveals 65% of eclipsed and 35% of staggered conformations because of positional disorder in one outer ethylene group. Central double C=C bond length analysis shows a similar intermediate 0.5+ charge on any of the four radical cations in the

α-layer: the corresponding C=C bond length values are 1.362(6), 1.378(6), 1.359(6) and 1.363(6) Å for E–H, respectively. Therefore, the regular structure and uniform charge state of the radical cations suggest that the α-layer could possess high conductivity. Note that the described charge distribution in the 'pseudo-κ' and α layers is observed both at room temperature and 120 K.

The anion layer is presented in Fig. 3. It has honeycomb-like arrangement with $[Fe(C_2O_4)_3]^{3-}$ anions and H_3O^+ cations alternating in vertexes of the hexagonal net. The large hexagonal cavities of the layer are filled by 1,2-dibromobenzene guest solvent molecules. The layer components are connected by strong hydrogen bonds (H···O distances less than 2.02 Å) between H_3O^+ cations and outer oxygen atoms of the oxalate ligands (see Fig. 3 and Table 1 for hydrogen bond geometries) and weaker H-bonds between anions and solvent molecules (the shortest H···O values shown in Fig. 3 are 2.47, 2.54 and 2.64 Å). Additionally, solvents are connected with the anions by shortened Br···O contacts of 3.230(3)–3.318(3) Å (Fig. 3).

It is clearly seen in the general structure view (Fig. 1) that all Br atoms of the solvent molecules (marked by filled circles in the anion layers) are directed towards the α-layer and participate in three shortened hydrogen contacts of C–H···Br type with outer ethylene fragments of the F and H radical cations, the corresponding H···Br distances being 2.61, 2.78 and 2.82 Å. For a comparison, similar hydrogen contacts between the anion layer and the 'pseudo-κ' layer exceed 2.98 Å. Additionally, hydroxonium cations also show asymmetrical disposition with respect to the α and 'pseudo-κ' layers: all the hydrogen atoms are directed towards the α-layer (H_3O^+ pyramids are marked out by black O–H bonds in Fig. 1). Concurrently, the anion oxygen atoms form a larger number of hydrogen bonds with BEDT-TTF molecules of the α-layer (13 bonds with H···O = 2.26–2.60 Å) as compared with the 'pseudo-κ' one (9 bonds with H···O = 2.37–2.57 Å). The asymmetrical location of the anion layer components with respect to two neighboring BEDT-TTF layers has a drastic influence on the layer packing and makes possible the coexistence in the crystal lattice of two conducting layers with non-equivalent structure and charge distribution. A conformable asymmetry of the anion layer was observed in another bi-layered phase of the family α-β″-$(BEDT\text{-}TTF)_4NH_4[M(C_2O_4)_3]\cdot G$ containing asymmetric (including chiral) guest solvents G.[9,14] Note, that in metallic α-β″-salts (which have M–I transition at 150–170 K) functional hydroxyl groups of the solvents are also located close to the α-layer surface like the Br-atoms of the 1,2-dibromobenzene solvent in our metallic α-'pseudo-κ' crystals. In contrast, in similar isostructural α-β″-salts which have non-metallic properties, polar –CO and –CN groups are displaced towards the β″-layer, as it has been mentioned by authors.[14]

Table 1 Geometry of hydrogen bonds formed between H_3O^+ and anion surrounding in the structure of α-'pseudo-κ'-$(BEDT\text{-}TTF)_4H_3O[Fe(C_2O_4)_3]C_6H_4Br_2$ at 120 K

H-bond[a]	D–H/Å	H···A/Å	D···A/Å	D–H···A/°
O(1w)–H(1a)···O(21)^{i}	1.11(3)	1.75(3)	2.834(5)	164(5)
O(1w)–H(1b)···O(11)^{ii}	1.11(3)	1.93(4)	2.942(5)	149(5)
O(1w)–H(1c)···O(7)	1.11(3)	1.84(3)	2.899(5)	156(5)
O(2w)–H(2a)···O(9)^{ii}	1.10(3)	1.72(3)	2.811(5)	171(5)
O(2w)–H(2b)···O(19)	1.11(3)	1.74(3)	2.835(5)	169(5)
O(2w)–H(2c)···O(23)^{ii}	1.12(3)	1.99(4)	2.953(5)	142(4)
O(2w)–H(2c)···O(24)^{ii}	1.12(3)	2.02(5)	2.878(5)	131(4)

[a] Symmetry operations: (i) x, $y + 1$, z and (ii) $x - 1$, y, z.

There are four series of salts in the $(BEDT\text{-}TTF)_4A^{I}[M^{III}(C_2O_4)_3]\cdot G$ family: monoclinic crystals with β″-type of BEDT-TTF layers, orthorhombic 'pseudo-κ', triclinic α-β″ and new triclinic α-'pseudo-κ' crystals. All of them have similar layered structure and honeycomb-like architecture of the anion layer with large hexagonal cavities incorporating different solvents. 1,2-Dibromobenzene has a molecular volume of approximately 170 Å^3 and appears to be the largest guest solvent molecule in the hexagonal anion network. It is interesting to compare the structural features of the new α-'pseudo-κ' crystals with those of all known phases of the family. As it is shown below, structural and electronic differences in the conducting BEDT-TTF layers originate from variations of anion layer composition and structure.

The three types of donor packing (β″, 'pseudo-κ' and α) in the $(BEDT\text{-}TTF)_4A^{I}[M^{III}(C_2O_4)_3]\cdot G$ family are presented schematically in Fig. 4a–c. Fig. 5 represents one hexagonal cell fragment of the anion layers in the monoclinic β″ (a), orthorhombic 'pseudo-κ' (b), novel triclinic α-'pseudo-κ' (c) and known triclinic α-β″ (d) phases. These phases differ, firstly, by distribution of right (Δ) and left (Λ) handed enantiomers of chiral

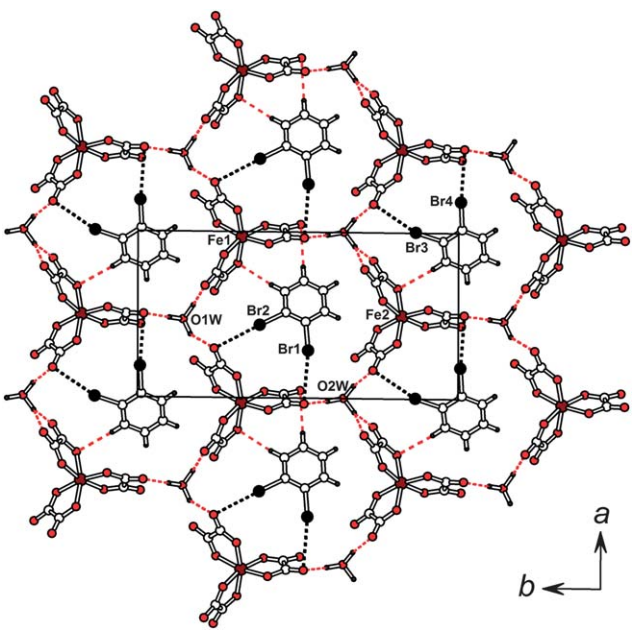

Fig. 3 Complex anion layer in the structure of α-'pseudo-κ'-$(BEDT\text{-}TTF)_4H_3O[Fe(C_2O_4)_3]C_6H_4Br_2$.

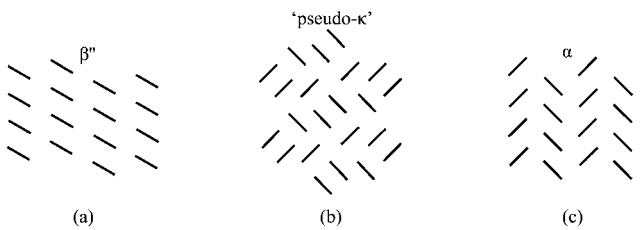

Fig. 4 Schematic view of different donor packing types in the $(BEDT\text{-}TTF)_4A^{I}[M^{III}(C_2O_4)_3]G$ family: (a) β″, (b) 'pseudo-κ' and (c) α.

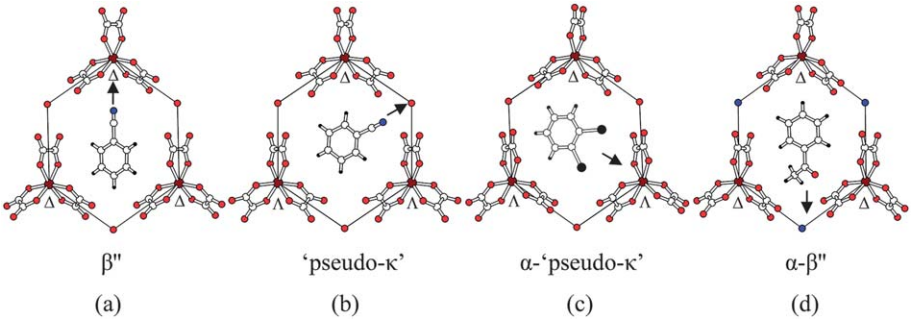

Fig. 5 Distinctions in solvent molecule arrangement in different phases of the (BEDT-TTF)$_4$A[Fe(C_2O_4)$_3$]G family: solvent molecule rotates (arrows show the direction of functional group for each phase) and phenyl ring shifts from the centre of the cavity in different directions. (Second orientation of disordered BN molecule in 'pseudo-κ' phase is omitted for clarity.)

$[M^{III}(C_2O_4)_3]^{3-}$ anion in the crystal lattice and, secondly, by solvent molecule orientation both within the hexagonal cavities and with respect to conducting BEDT-TTF layers. By arrangement of Δ- and Λ-[Fe(C_2O_4)]$^{3-}$, the anion layer of triclinic α-'pseudo-κ' crystals is close to the orthorhombic pure 'pseudo-κ' phase of the family, since both of these phases contain mixture of two enantiomers in each anion layer (Fig. 5b and c), while in the bi-layered α-β″-salts, as in the pure β″-phase, every anion layer is chiral and the layers made from only right or only left handed anion isomers alternate along the *c*-axis (Fig. 5a and d). Every phase has a characteristic intrinsic orientation of the guest solvent molecules G inside the anion layer cavity, all possible orientations of functional groups attached to phenyl ring being realized (Fig. 5).

Interestingly, the conducting BEDT-TTF layer of α-type appears to have a large ability for adapting itself to both chiral and racemic anion layers. The hexagonal cavity area in the anion networks remains almost constant and amounts to 103 ± 1 Å^2 in all the crystals of the family, although hexagons can be distorted and M^{III}–A^+ distances change within the limits of 6.2–6.4 Å. However, the mutual arrangement of subsequent anion layers varies significantly in different phases. Fig. 6 demonstrates that alternating anion layers in all the crystals are related by inversion, but the direction and magnitude of their relative displacement within the layer plane are non-equivalent when the anion layers interface with donor layers of different types. It is found that mutual relations of both β″ and 'pseudo-κ' donor layers with anion layers (relative orientation, interlayer molecular contacts and so on) in the mixed α-β″ and α-'pseudo-κ' remains essentially the same as in the corresponding pure β″ and 'pseudo-κ' phases (Fig. 6a and b). Therefore, one can conclude that stable combinations Δ-β″-Λ and (Δ + Λ)-'pseudo-κ'-(Δ + Λ) behave as robust structural blocks during the crystallization process. In contrast, the α-layer plays a more dependent role and joins the blocks, integrating between two anion layers in two different ways and forming combinations (Δ + Λ)-α-(Δ + Λ) in the α-'pseudo-κ' phase or Δ-α-Λ in α-β″ crystals (Fig. 6c and d, respectively). Thus, the α-packing motif appears to be more flexible and resistant to observed structural modifications in metalloxalate anion layer.

In general, structures with dual packing motifs rarely occur in organic molecular conductors. Among the BEDT-TTF-based compounds, there are five salts with tris(oxalato)metallate anions described above: α-β″-(BEDT-TTF)$_4$NH$_4$[M(C_2O_4)$_3$]·G with M/G = Ga/PhN(CH_3)COH (**1**), Ga/PhCH_2CN (**2**), Fe/PhCOCH_3 (**3**),[9] Fe/(*X*)–PhCOH(H)CH_3 with *X* = *R*/*S* (**4**) or *S* (**5**);[14] and five salts with other anions: β″-β-(BEDT-TTF)$_3$(MCl_4)$_2$ where M = Zn (**6**)[27] and Mn (**7**),[28] β″-θ-(BEDT-TTF)$_2$C(SO_2CF_3)$_3$ (**8**),[29] α-κ-(BEDT-TTF)$_2$Hg(SCN)$_3$ (**9**)[30] and κ-δ-(BEDT-TTF)$_2$Ag(CF_3)$_4$·$C_2H_3Cl_3$ (**10**).[31] Crystals of **1**, **2**, **6** and **7** are semiconductors while **4**, **5**, **8** and **9** show metal-to-insulator transition at rather high temperatures: 150 K (**4**), 170 K (**5**), 180–240 K (**8**) and 176 K (**9**). **10** is a first bi-layered organic superconductor with two-step superconducting transition (T_{C1} = 11.1 K, T_{C2} = 9.2 K). The salt **9** is closer to the title compound by architecture of the BEDT-TTF layers. However, noticeable

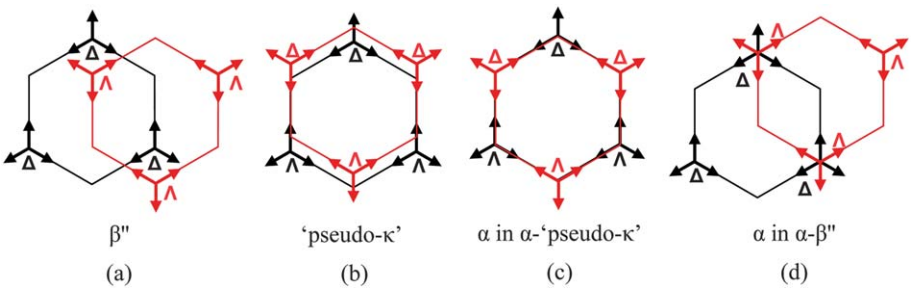

Fig. 6 Schemes of mutual orientation of two subsequent anion layers on the frontier of the: (a) β″ layer in pure β″ and mixed α-β″ phases, (b) 'pseudo-κ' layer in pure 'pseudo-κ' and mixed α-'pseudo-κ' phases, (c) α layer in α-'pseudo-κ' phase and (d) α layer in the α-β″ phase. Adjacent anion layers on the projections along the *c**-axis are shown by black and red colors; anions are shown schematically: arrows indicate directions of the oxalate ligands. Right and left enantiomers of the chiral [Fe(C_2O_4)]$^{3-}$ anion are labeled by symbols Δ and Λ, respectively.

difference is observed in the internal structure of the metallic α-layers: dihedral angles between molecules from the adjacent stacks are 46° in **9** and 87° in the new α-'pseudo-κ' salt. Besides, structure **9** is unstable and the crystal undergoes a sharp first-order structural transition at 176 K which leads to transfer from metallic to insulating states. α-'pseudo-κ'-(BEDT-TTF)$_4$H$_3$O[Fe(C$_2$O$_4$)$_3$]·C$_6$H$_4$Br$_2$, in contrast to most bi-layered BEDT-TTF conductors, has stable metallic and structural properties until liquid helium temperatures.

Electronic band structure

The 'pseudo-κ' layer. The band structure for the 'pseudo-κ' layer is shown in Fig. 7a. There are eight bands based on the HOMO of BEDT-TTF and the two upper bands are well separated from the other. With four holes in these bands, as expected from the stoichiometric formula and assuming an equal number of electrons in the two donor layers, a clear band gap is associated with the 'pseudo-κ' layers.

Shown in Fig. 7b is the density of states (DOSs) associated with the HOMO bands of Fig. 7a. The projected DOSs of the HOMOs of the A and C donors as well as those of the B and D donors are shown in Fig. 7c. The contribution of the HOMOs of A and C is separated in two main components associated with the bonding (lower) and antibonding (upper) combinations of the two HOMOs of each dimer. The bonding combination interacts a little bit with the HOMOs of the B and D molecules so that some portion of this contribution appears in the region of the

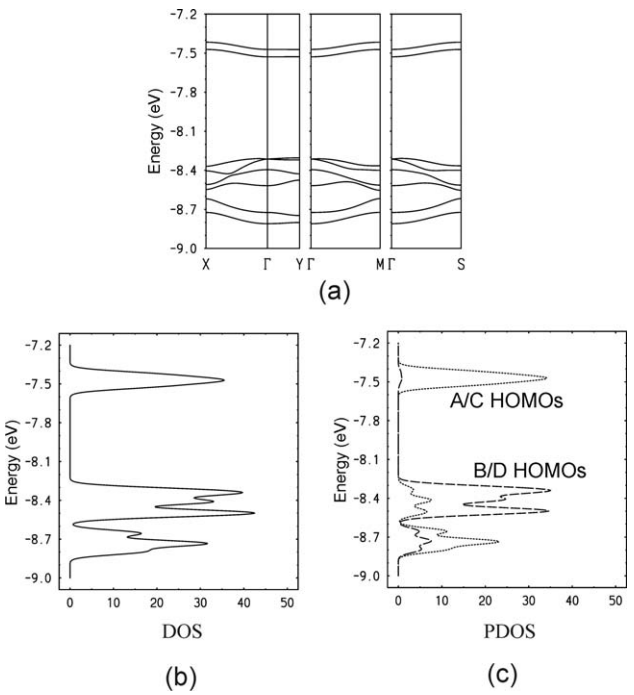

Fig. 7 The 'pseudo-κ' donor layer of α-'pseudo-κ'-(BEDT-TTF)$_4$H$_3$O[Fe(C$_2$O$_4$)$_3$]C$_6$H$_4$Br$_2$ at 120 K: (a) calculated band structure where $\Gamma = (0, 0)$, $X = (a^*/2, 0)$, $Y = (0, b^*/2)$, $M = (a^*/2, b^*/2)$ and $S = (-a^*/2, b^*/2)$; (b) calculated density of states (in units of electrons per eV and unit cell) in the region of the HOMO bands; and (c) projected density of states (PDOS) of the HOMOs of the A and C donors (dotted line) and the B and D donors (dashed line).

HOMOs of the neutral donors whereas the antibonding combinations remain isolated. These results, suggesting charges of +1 for donors A/C and 0 for donors B/D, are in complete agreement with the analysis of the central C=C bond lengths of the donors. It is clear that the dimerization of the A and C donors leads to a strong splitting of the HOMO levels and thus the 'pseudo-κ' layer should be associated with an activated conductivity.

The α layer. The α layers contain four different donors and fourteen different interactions, six of them (I to VI) are intrastack interactions and eight are interstack interactions. The HOMOs of the four donors are very similar in energy lying within a narrow energy range of 0.05 eV. Thus, if the overlap is not very weak it is expected that the four HOMOs interact quite strongly to lead to the eight HOMO based bands. The different interactions are defined in Fig. 2b and the calculated $|\beta_{HOMO-HOMO}|$ values[32] for every type of HOMO···HOMO interaction as well as the S···S contacts smaller than 4.0 Å are given in Table 2.

It is clear from Table 2 that practically all interactions are quite substantial so that these layers can be described as a two-dimensional net of interacting HOMOs. The values of Table 2 show some important differences with the case of the well known α-(BEDT-TTF)$_2$MHg(SCN)$_4$ phases. For instance, the $|\beta_{HOMO-HOMO}|$ values for the α-(BEDT-TTF)$_2$KHg(SCN)$_4$ phase are 0.242, 0.147, 0.240 and 0.157 eV for the interstack interactions and 0.060, 0.060, 0.014 and 0.169 eV for the intrastack interactions (note that the unit cell in this case contains only four donors). Thus, whereas practically all interstack interactions are nearly equal to or large than 0.2 eV in the present salt, this is the case for only half of the interactions in α-(BEDT-TTF)$_2$KHg(SCN)$_4$. The larger values as well as the uniformity of interactions lead to globally stronger interstack interactions in the present salt. More important is the difference concerning the intrastack interactions. In the α-(BEDT-TTF)$_2$MHg(SCN)$_4$ phases one of the chains exhibits a strong dimerization (0.169/

Table 2 Calculated values of the $|\beta_{HOMO-HOMO}|$ [eV] for the different donor···donor interactions and S···S contacts smaller than 4.0 Å for the α layer of α-'pseudo-κ'-(BEDT-TTF)$_4$H$_3$O[Fe(C$_2$O$_4$)$_3$]C$_6$H$_4$Br$_2$ at 120 K

Interaction	S···S/Å	$\|\beta_{HOMO-HOMO}\|$/eV
I	[4.048(×2), 4.005(×2)]	0.1116
II	3.720, 3.773, 3.775, 3.851	0.1332
III	3.751(×2), 3.884(×2)	0.1458
IV	3.712, 3.721, 3.785, 3.839	0.2079
V	3.867(×2), 3.986(×2)	0.0682
VI	3.930(×2), 3.931(×2)	0.1140
VII	3.546, 3.649, 3.705, 3.742, 3.873, 3.920, 3.989	0.1737
VIII	3.531, 3.551, 3.581, 3.784, 3.797, 3.874	0.2184
IX	3.619, 3.710, 3.711, 3.783, 3.889, 3.932, 3.967	0.1845
X	3.475, 3.537, 3.555, 3.736, 3.859, 3.864, 3.906	0.2030
XI	3.468, 3.547, 3.630, 3.631, 3.772, 3.788	0.2378
XII	3.550, 3.566, 3.604, 3.689, 3.743, 3.906, 3.982	0.2391
XIII	3.423, 3.619, 3.695, 3.730, 3.923	0.2098
XIV	3.435, 3.489, 3.627, 3.769, 3.785, 3.921, 3.944	0.2063

0.014 in α-(BEDT-TTF)$_2$KHg(SCN)$_4$) with one of the interactions being very weak. This means that one of the two stacks must be considered as a stack of dimers in weak interaction. This is not the case in the present salt. The interactions in the second type of stacks in the α-(BEDT-TTF)$_2$MHg(SCN)$_4$ phases are considerably weaker than the interstack interactions. In the present case the difference is smaller. These two differences are at the origin of a very different type of band structure for the two types of α phases. Whereas for the α-(BEDT-TTF)$_2$MHg(SCN)$_4$ family it was shown that the partially filled bands could be considered to result from the interaction of chains of alternating dimers and monomers along the direction perpendicular to the stacks,[19] the stronger intrastack interactions and the absence of strong dimerization make such description non-applicable to the present salt. Here practically all interactions are substantial so that the layers are expected to be strongly two-dimensional systems and thus, exhibit a band structure and Fermi surface completely different from those of the α-(BEDT-TTF)$_2$MHg(SCN)$_4$ family.

This analysis is completely confirmed by the calculated band structure (Fig. 8a) and Fermi surface (Fig. 8b) for the α layers of the present salt. For instance, the Fermi surface contains a series of closed portions which correspond to a 2D metal. Those centered at M correspond to holes and have an area which is twice that of the two equivalent pseudo-triangular electron pockets. This Fermi surface does not exhibit any nesting property so that the metallic state is expected to be stable until low temperatures.

The calculated area of the hole and electron pockets in Fig. 8b is 7.6% and 3.8% of the cross-section of the Brillouin zone, respectively. Consequently, the system is expected to exhibit two different Shubnikov–de Haas (SdH) frequencies, one being half of the other. In addition we note that the Fermi level just touches a third band at M so that it is possible that small changes in pressure and temperature could lead to a third and small closed pocket in the Fermi surface corresponding to holes. In that case there should be three different SdH frequencies in such a way that twice the frequency of the intermediate frequency should be equal to the sum of the large and small frequencies.

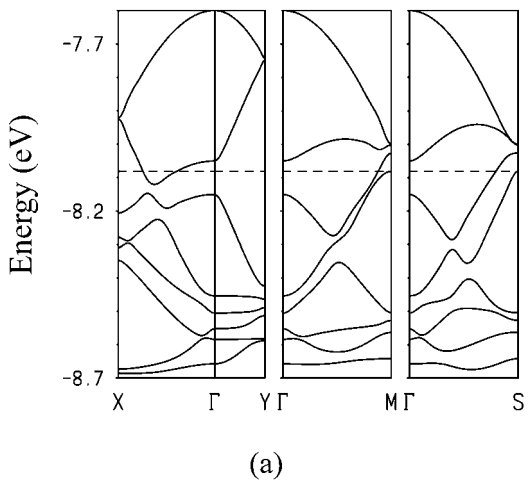

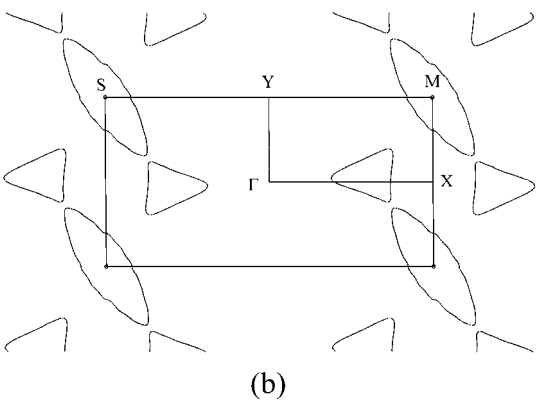

Fig. 8 The α layer of α-'pseudo-κ'-(BEDT-TTF)$_4$H$_3$O[Fe(C$_2$O$_4$)$_3$]C$_6$H$_4$Br$_2$ at 120 K: (a) calculated band structure where the dashed line refers to the Fermi level and $\Gamma = (0, 0)$, $X = (a^*/2, 0)$, $Y = (0, b^*/2)$, $M = (a^*/2, b^*/2)$ and $S = (-a^*/2, b^*/2)$; (b) calculated Fermi surface.

Magnetotransport properties

The metallic-like temperature dependence of the sample resistance was observed down to 0.4 K (Fig. 9). The curve $\rho_\perp(T)$ is very similar to that obtained earlier (see Fig. 7 in ref. 18). Some difference in the shape of the curve appears, probably, owing to the different sample qualities: the amplitude of the "hump" due to the coherent–incoherent transition in the out-of-plane transport in the layered highly anisotropic crystals is known to be sensitive to the impurity scattering.[33,34]

The results of the magnetoresistance measurements are presented in Fig. 10. At $B > 8$ T well pronounced SdH oscillations are observed. The oscillation period in 1/B scale corresponds to the Fermi surface cross-section $S = 1.75 \times 10^{18}$ m^{-2} which is 8.94% of the Brillouin zone square. This value coincides fairly well with the calculated cross-section of the hole pockets. No other SdH oscillation frequencies were registered in this magnetic field range. From the temperature dependence of the oscillation amplitude (see Fig. 11) the value of the cyclotron mass $m_c = 1.26m_e$ (where m_e is the free electron mass) was obtained using the standard Lifshitz–Kosevich analysis.[35] The reason why we

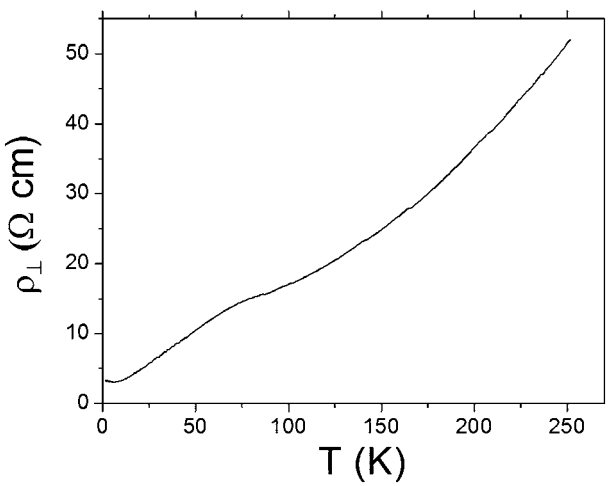

Fig. 9 Temperature dependence of the out-of-plane resistivity of α-'pseudo-κ'-(BEDT-TTF)$_4$H$_3$O[Fe(C$_2$O$_4$)$_3$]C$_6$H$_4$Br$_2$ single crystal.

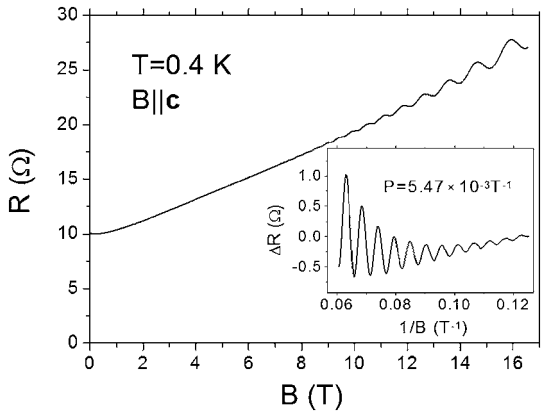

Fig. 10 The magnetic field dependence of the sample out-of-plane resistance at 0.4 K. In the inset: SdH oscillations in $1/B$ scale, the linear part of $R(B)$ dependence is subtracted.

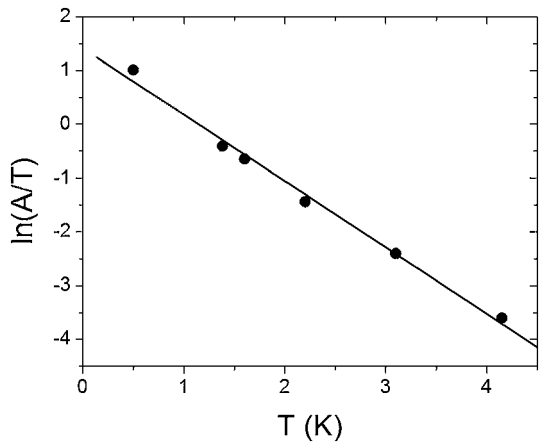

Fig. 11 The plot ln (A/T) *versus* T; A—the oscillation amplitude at $B =$ 15.1 T. The slope of the straight line gives the cyclotron effective mass $m_c/m_e = 1.26$, m_e—free electron mass.

did not observe the oscillations corresponding to the electron pockets is not yet clear although it is likely that one needs much higher magnetic fields to observe them.

Conclusion

In summary, α-'pseudo-κ'-(BEDT-TTF)$_4$H$_3$O[Fe(C$_2$O$_4$)$_3$]·C$_6$H$_4$Br$_2$ is the first radical cation salt with alternating α and 'pseudo-κ' organic BEDT-TTF layers. Remarkably, the two layers have a pronounced difference in conducting properties: the layer of the α-type is composed of uniform stacks of equally charged BEDT-TTF$^{0.5+}$ radical cations and has metallic properties and the Fermi surface does not exhibit nesting properties leading to a stable metallic behavior of the crystals down to 0.4 K, whereas the 'pseudo-κ'-layer is characterized by the strong charge disproportionation between (BEDT-TTF$^+$)$_2$ dimers and BEDT-TTF^0 monomers, and the observed charge localization unambiguously corresponds to activated conductivity.

Comparative analysis of the structures of four different salts of the (BEDT-TTF)$_4$A^{I}[M^{III}(C$_2$O$_4$)$_3$]G family (monoclinic β″, orthorhombic 'pseudo-κ', known triclinic α-β″ and novel triclinic α-'pseudo-κ') shows a number of important distinctions between all the phases. In particular, packing types of conducting layers, arrangement of chiral [Fe(C$_2$O$_4$)$_3$]$^{3-}$ anions in racemic crystals, orientation of solvent molecules inside the anion layer and relative disposition of the adjacent anion sheets on the interface of various donor layers are shown to be different. Certain combinations of donor and anion layers Δ-β″-Λ and (Δ + Λ)-'pseudo-κ'-(Δ + Λ) are found to be robust structural blocks stable in different phases, while the α packing mode of BEDT-TTF radical cations is more flexible and can adapt itself to anion layers of different geometries leading as a result to combinations (Δ + Λ)-α-(Δ + Λ) or Δ-α-Λ.

The α-'pseudo-κ'-(BEDT-TTF)$_4$H$_3$O[Fe(C$_2$O$_4$)$_3$]·C$_6$H$_4$Br$_2$ compound is a really two-dimensional system in which thin metallic sheets (α-layers of about 14 Å) are separated by the thicker insulating "gaskets" (about 22 Å) comprising 'pseudo-κ'-(BEDT-TTF) layer and two anion layers. Electronic band structure calculations confirm the 2D metallic nature of the α layer along with non-metallic properties of the 'pseudo-κ' layer. However, the calculated Fermi surface of the α-layer in the α-'pseudo-κ'-salt is completely different from that in the well known α-(BEDT-TTF)$_2$MHg(SCN)$_4$ family of organic metals and superconductors. Shubnikov–de Haas oscillations of the magnetoresistance have been observed in the α-'pseudo-κ'-(BEDT-TTF)$_4$H$_3$O[Fe(C$_2$O$_4$)$_3$]·C$_6$H$_4$Br$_2$ crystal at $B > 8$ T. The theoretically predicted cross-section area of the hole pocket in Fermi surface is in a good agreement with the experimentally measured SdH oscillation period.

Acknowledgements

This work was partially supported by the RFBR grants 09-02-00241, 09-02-00852 and the Program of Russian Academy of Sciences. Work at Bellaterra was supported by DGES-Spain (Projects FIS2009-12721-C04-03 and CSD2007-00041).

References

1 M. Kurmoo, A. W. Graham, P. Day, S. J. Coles, M. B. Hursthouse, J. L. Caufield, J. Singleton, F. L. Pratt, W. Hayes, L. Ducasse and P. Guionneau, *J. Am. Chem. Soc.*, 1995, **117**, 12209.
2 L. Martin, S. S. Turner, P. Day, F. E. Mabbs and J. L. McInnes, *Chem. Commun.*, 1997, 1367.
3 S. S. Turner, P. Day, K. M. Abdul Malik, M. B. Hursthouse, S. J. Teat, E. J. MacLean, L. Martin and S. A. French, *Inorg. Chem.*, 1999, **38**, 3543.
4 L. Martin, S. S. Turner, P. Day, P. Guionneau, J. A. K. Howard, D. E. Hibbs, M. E. Light, M. B. Hursthouse, M. Uruichi and K. Yakushi, *Inorg. Chem.*, 2001, **40**, 1363.
5 S. Rashid, S. S. Turner, P. Day, J. A. K. Howard, P. Guionneau, E. J. L. McInnes, F. E. Mabbs, R. J. H. Clark, S. Firth and T. Biggse, *J. Mater. Chem.*, 2001, **11**, 2095.
6 S. Rashid, S. S. Turner, D. Le Pevelen, P. Day, M. E. Light, M. B. Hursthouse, S. Firth and R. J. H. Clark, *Inorg. Chem.*, 2001, **40**, 5304.
7 T. G. Prokhorova, S. S. Khasanov, L. V. Zorina, L. I. Buravov, V. A. Tkacheva, A. A. Baskakov, R. B. Morgunov, M. Gener, E. Canadell, R. P. Shibaeva and E. B. Yagubskii, *Adv. Funct. Mater.*, 2003, **13**, 403.
8 A. Audouard, V. N. Laukhin, L. Brossard, T. G. Prokhorova, E. B. Yagubskii and E. Canadell, *Phys. Rev. B: Condens. Matter Mater. Phys.*, 2004, **69**, 144523.
9 H. Akutsu, A. Akutsu-Sato, S. S. Turner, P. Day, E. Canadell, S. Firth, R. J. N. Clark, J. Yamada and S. Nakatsuji, *Chem. Commun.*, 2004, 18.

10 E. Coronado and P. Day, *Chem. Rev.*, 2004, **104**, 5419.
11 A. Akutsu-Saito, A. Kobayashi, T. Mori, H. Akutsu, J. Yamada, S. Nakatsuji, S. S. Turner, P. Day, D. A. Tocher, M. E. Light and M. B. Hursthouse, *Synth. Met.*, 2005, **152**, 373.
12 E. Coronado, S. Curelli, C. Giménez-Saiz and C. J. Gómez-García, *Synth. Met.*, 2005, **154**, 245.
13 E. Coronado, S. Curelli, C. Giménez-Saiz and C. J. Gómez-García, *J. Mater. Chem.*, 2005, **15**, 1429.
14 L. Martin, P. Day, H. Akutsu, J. Yamada, S. Nakatsuji, W. Clegg, R. W. Harrington, P. N. Horton, M. B. Hursthouse, P. McMillan and S. Firth, *CrystEngComm*, 2007, **9**, 865.
15 A. Akutsu-Sato, H. Akutsu, J. Yamada, S. Nakatsuji, S. S. Turner and P. Day, *J. Mater. Chem.*, 2007, **17**, 2497.
16 L. V. Zorina, T. G. Prokhorova, S. V. Simonov, S. S. Khasanov, R. P. Shibaeva, A. I. Manakov, V. N. Zverev, L. I. Buravov and E. B. Yagubskii, *J. Exp. Theor. Phys.*, 2008, **106**, 347.
17 C. J. Gómez-García, B. Rahman, C. Giménez-Saiz and E. Coronado, *International Conference on Science and Technology of Synthetic Metals 2010 (ICSM-2010)*, Kyoto, Japan, July 4–9, 2010, Abstract Book, p. 205.
18 T. G. Prokhorova, L. I. Buravov, E. B. Yagubskii, L. V. Zorina, S. S. Khasanov, S. V. Simonov, R. P. Shibaeva, A. V. Korobenko and V. N. Zverev, *CrystEngComm*, 2011, **13**, 537.
19 R. Rousseau, M.-L. Doublet, E. Canadell, R. P. Shibaeva, S. S. Khasanov, L. P. Rozenberg, N. D. Kushch and E. B. Yagubskii, *J. Phys. I*, 1996, **6**, 1527.
20 M. V. Kartsovnik, *Chem. Rev.*, 2004, **104**, 5737.
21 Oxford Diffraction, *Xcalibur CCD System, CrysAlisPro Software System, Version 1.171.32*, Oxford Diffraction Ltd., 2007.
22 G. M. Sheldrick, *Acta Crystallogr., Sect. A: Found. Crystallogr.*, 2008, **64**, 112.
23 M.-H. Whangbo and R. Hoffmann, *J. Am. Chem. Soc.*, 1978, **100**, 6093.
24 J. H. Ammeter, H.-B. Bürgi, J. Thibeault and R. Hoffmann, *J. Am. Chem. Soc.*, 1978, **100**, 3686.
25 A. Pénicaud, K. Boubekeur, P. Batail, E. Canadell, P. Auban-Senzier and D. Jérome, *J. Am. Chem. Soc.*, 1993, **115**, 4101.
26 A. Pénicaud, P. Batail, C. Coulon, E. Canadell and C. Perrin, *Chem. Mater.*, 1990, **2**, 123.
27 V. E. Korotkov and R. P. Shibaeva, *Sov. Phys. Crystallogr.*, 1989, **34**, 865.
28 T. Mori and H. Inokuchi, *Bull. Chem. Soc. Jpn.*, 1988, **61**, 591.
29 J. A. Schlueter, U. Geiser, H. H. Wang, A. M. Kini, B. H. Ward, J. P. Parakka, R. G. Daugherty, M. E. Kelly, P. G. Nixon, G. L. Gard, L. K. Montgomery, H.-J. Koo and M.-H. Whangbo, *J. Solid State Chem.*, 2002, **168**, 524.
30 J. A. Schlueter, U. Geiser, M. A. Whited, N. Drichko, B. Salameh, K. Petukhov and M. Dressel, *Dalton Trans.*, 2007, 2580.
31 J. A. Schlueter, L. Wiehl, H. Park, M. de Souza, M. Lang, H.-J. Koo and M.-H. Whangbo, *J. Am. Chem. Soc.*, 2010, **132**, 16308.
32 M.-H. Whangbo, J. M. Williams, P. C. W. Leung, M. A. Beno, T. J. Emge and H. H. Wang, *Inorg. Chem.*, 1985, **24**, 3500.
33 D. B. Gutman and D. L. Maslov, *Phys. Rev. Lett.*, 2007, **99**, 196602.
34 J. G. Analytis, A. Ardavan, S. J. Blundell, R. L. Owen, E. F. Garman, C. Jeynes and B. J. Powell, *Phys. Rev. Lett.*, 2006, **96**, 177702.
35 D. Shoenberg, *Magnetic Oscillations in Metals*, Cambridge University Press, Cambridge, 1984.

